



# Pd Doped on TCH@SBA-15 Nanocomposites: Fabrication and Application as a New Organometallic Catalyst in the Three-Component Synthesis of *N*-Benzo-imidazo- or -thiazole-1,3-thiazolidinones

Mehdi Kalhor\* and Akbar Dadras

Department of Chemistry, Payame Noor University, Tehran, Iran

## OPEN ACCESS

### Edited by:

Masoud Mokhtary,  
Islamic Azad University, Rasht  
Branch, Iran

### Reviewed by:

Alain Rafael Puente Santiago,  
The University of Texas at El Paso,  
United States  
Taiebeh Tamoradi,  
Production Technology Research  
Institute-ACECR, Ahvaz, Iran

### \*Correspondence:

Mehdi Kalhor  
mekalhor@gmail.com

### Specialty section:

This article was submitted to  
Organic Chemistry,  
a section of the journal  
Frontiers in Chemistry

Received: 10 June 2021

Accepted: 19 August 2021

Published: 04 October 2021

### Citation:

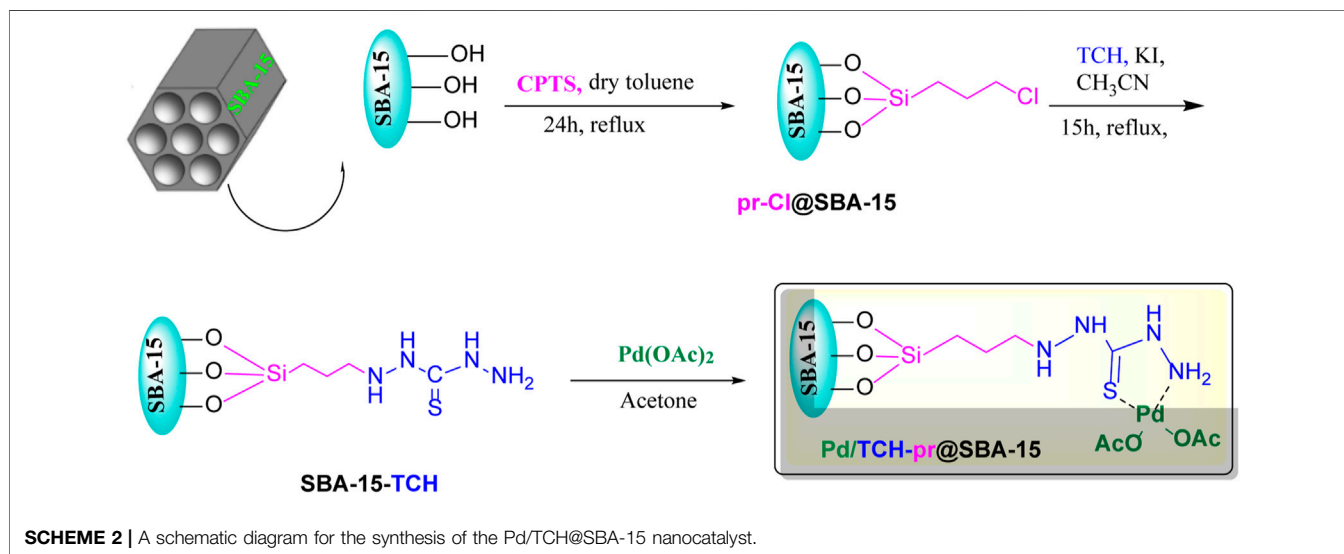
Kalhor M and Dadras A (2021) Pd  
Doped on TCH@SBA-15  
Nanocomposites: Fabrication and  
Application as a New Organometallic  
Catalyst in the Three-Component  
Synthesis of *N*-Benzo-imidazo- or -  
thiazole-1,3-thiazolidinones.  
Front. Chem. 9:723207.  
doi: 10.3389/fchem.2021.723207

In this study, Pd(II)/TCH@SBA-15 nanocomposites were synthesized by the grafting of 3-chloropropyltriethoxysilane and thiocarbonylhydrazide on SBA-15 and subsequent deposition of palladium acetates through the ligand–metal coordination method. The structure and morphology of this nanoporous nanocomposite was thoroughly identified by Fourier transform infrared spectroscopy, field emission scanning electron microscopy, transmission electron microscopy, energy-dispersive X-ray spectroscopy, X-ray diffraction, thermogravimetric analysis, atomic absorption spectroscopy, and Brunauer–Emmett–Teller instrumental analyses. Furthermore, the catalytic activity of this nanocomposite was investigated in the three-component synthesis of 3-benzimidazolyl or benzothiazole-1,3-thiazolidin-4-ones via a reaction of 2-aminobenzimidazole or 2-aminobenzothiazole, aromatic aldehydes, and thioglycolic acid in an acetone–H<sub>2</sub>O mixture under green conditions. The Pd/TCH@SBA-15 nanocatalyst is demonstrated to exhibit a high catalyzing activity in the three-component reaction of the synthesis of *N*-heterocyclic thiazolidinones with good to excellent yields. One of the advantages of the suggested method is the direct application of the thiocarbonylhydrazide ligand to stabilize Pd nanoparticles through formation of a stable ring complex without creating an additional Schiff base step. Moreover, this organometallic nanocatalyst can be recycled several times with no notable leaching or loss of performance.

**Keywords:** Pd@SBA-15, organometallic nanocatalyst, thiocarbonylhydrazide, three-component reaction, 2-aminobenzimidazole, 2-aminobenzothiazole, 1,3-thiazolidinone

## INTRODUCTION

Today, continuous efforts are made to place organometallic functional groups on heterogeneous supports and apply them in catalytic reactions. Supported catalysts have both homogeneous and heterogeneous catalytic benefits (Wan and Zhao, 2007; Muñoz-Batista et al., 2018; Rodríguez-Padrón et al., 2019; Rodríguez-Padrón et al., 2019; Tamoradi et al., 2020). Among the suitable supports, SBA-15 silicate has received considerable attention due to its desirable properties such as



regular channel nanostructures, a pore diameter in the range of 2–30 nm, a high surface-to-volume ratio, suitable selectivity, high thermal and mechanical stability, and adjustable surface chemistry (Zhao et al., 1998; Fulvio et al., 2005; Ostovar et al., 2018; Rajabi et al., 2019). In addition, the ability to design, manipulate, and modify the surface of SBA-15 by organic and inorganic materials due to large amounts of surface hydroxyl groups, which is a key factor for its application in catalytic processes, has led to special attention to these porous structures (Feng et al., 2010; Bhuyan et al., 2015; Ostovar et al., 2018). One of the convenient procedures for applying SBA-15 nanoparticles as a catalyst is to anchor the desired functional groups on high surface mesoporous silica. In these cases, a covalent interaction could be established between the organic functional group and the silica framework, which prevents leaching of the active sites into the reaction mixture after repeated use. Therefore, heterogeneous catalysts with active metal centers supported on SBA-15-modified nanoparticles could be an ideal option in catalytic systems (Karimi et al., 2006).

Pd species are one of the most versatile catalysts used in modern organic synthesis and have been widely used in a significant number of synthetic transformations (Kim et al., 2012; Veisi et al., 2019) and cross-couplings and related reactions, such as Heck, Suzuki, Stille, and Sonogashira types (Calo et al., 2005; Tamami et al., 2011; Biffis et al., 2018; Veisi

et al., 2019; Tamoradi et al., 2020; Veisi et al., 2020). So far, several reviews have been reported on the role of Pd as a metal catalyst with or without support in classical and modern organic reactions (Lamblin et al., 2010; Molnár, 2011; Biffis et al., 2018; Veisi et al., 2020). Pd salts or complexes, preformed or produced *in situ* upon addition of a ligand, are commonly utilized as sources of palladium for these reactions. It is known that well-dispersed Pd catalysts immobilized on suitable supports, such as the SBA-15, can enhance their catalytic activity. Finally, the development of a new and efficient approach for the stabilization of Pd nanoparticles onto the SBA-15 surface as organometallic materials is still needed for catalytic organic transformation.

1,3-Thiazolidine-4-ones with sulfur and nitrogen atoms and a carbonyl group in a 5-membered ring belong to a large family of thiazoles, which are of special importance and attention due to their extensive activities in the biological, pharmaceutical, and agricultural fields (Cunico et al., 2008; Mobinikhaledi et al., 2010; Jain et al., 2012; Zhang et al., 2020). The basic component of thiazolidinone has been used in the structure of various important drugs, such as thiazolidomycin (antibiotic), ralitoline (antiepileptic), rosiglitazone (antidiabetic), and etozoline (loop diuretic). This widespread application highlights the importance of access to effective synthetic pathways for the production of thiazolidine-4-one compounds. The general method of synthesis can be either a one-pot or a two-

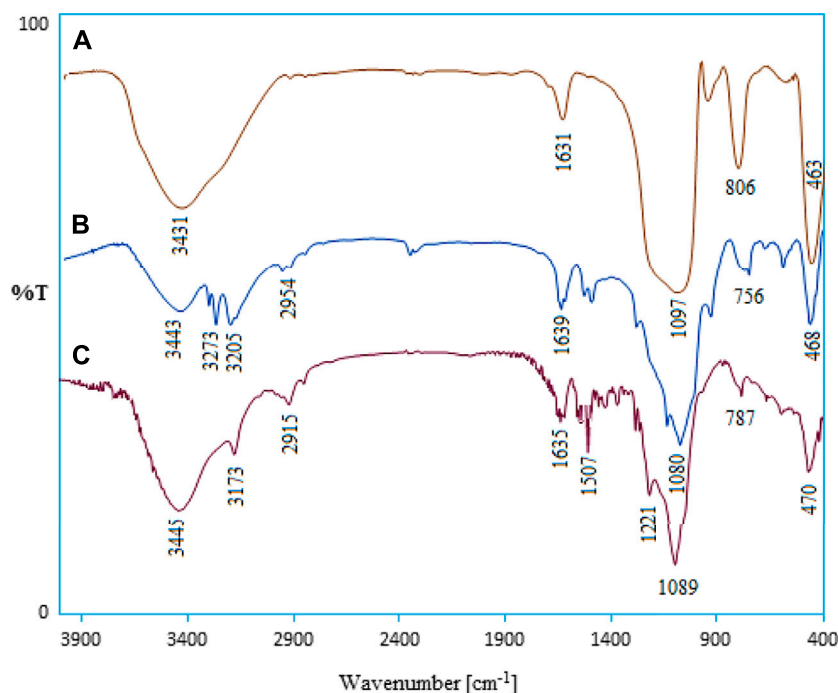


**FIGURE 1** | FT-IR spectra of (A) SBA-15, (B) SBA-15-TCH, and (C) Pd/TCH@SBA-15.

step process of an amine with aromatic aldehydes and thioglycolic acid, under traditional hard conditions, or with the use of heterogeneous and homogenous catalysts (Srivastava et al., 2001; Kumar et al., 2013; Thakare et al., 2014; Jadhav et al., 2015; Chate et al., 2016; Harale et al., 2016; Pang et al., 2016; Safaei-Ghomi et al., 2016; Safaei-Ghomi et al., 2016; Thakare et al., 2016; Kalhor et al., 2017; Kalhor et al., 2018; Kalhor and Banibairami, 2020). However, despite reports of good progress in the synthesis of these valuable compounds, there are still some limitations to these methods and research and development to achieve new, more efficient, and greener synthetic strategies is useful and in demand.

Considering the above points in our ongoing research on the synthesis of organometallic nanocatalysts (Kalhor et al., 2019; Kalhor et al., 2020), we report herein a simple method for the preparation of stable and active Pd supported on TCH@SBA-15 mesoporous composites as a nanocatalyst for the three-component synthesis of 2-aryl-*N*-benzo-imidazo- or -thiazole-1,3-thiazolidinones *via* condensation of the aldehyde derivatives 2-aminobenzimidazole or benzothiazole and thioglycolic acid under green conditions (Scheme 1).

## EXPERIMENTAL METHODS

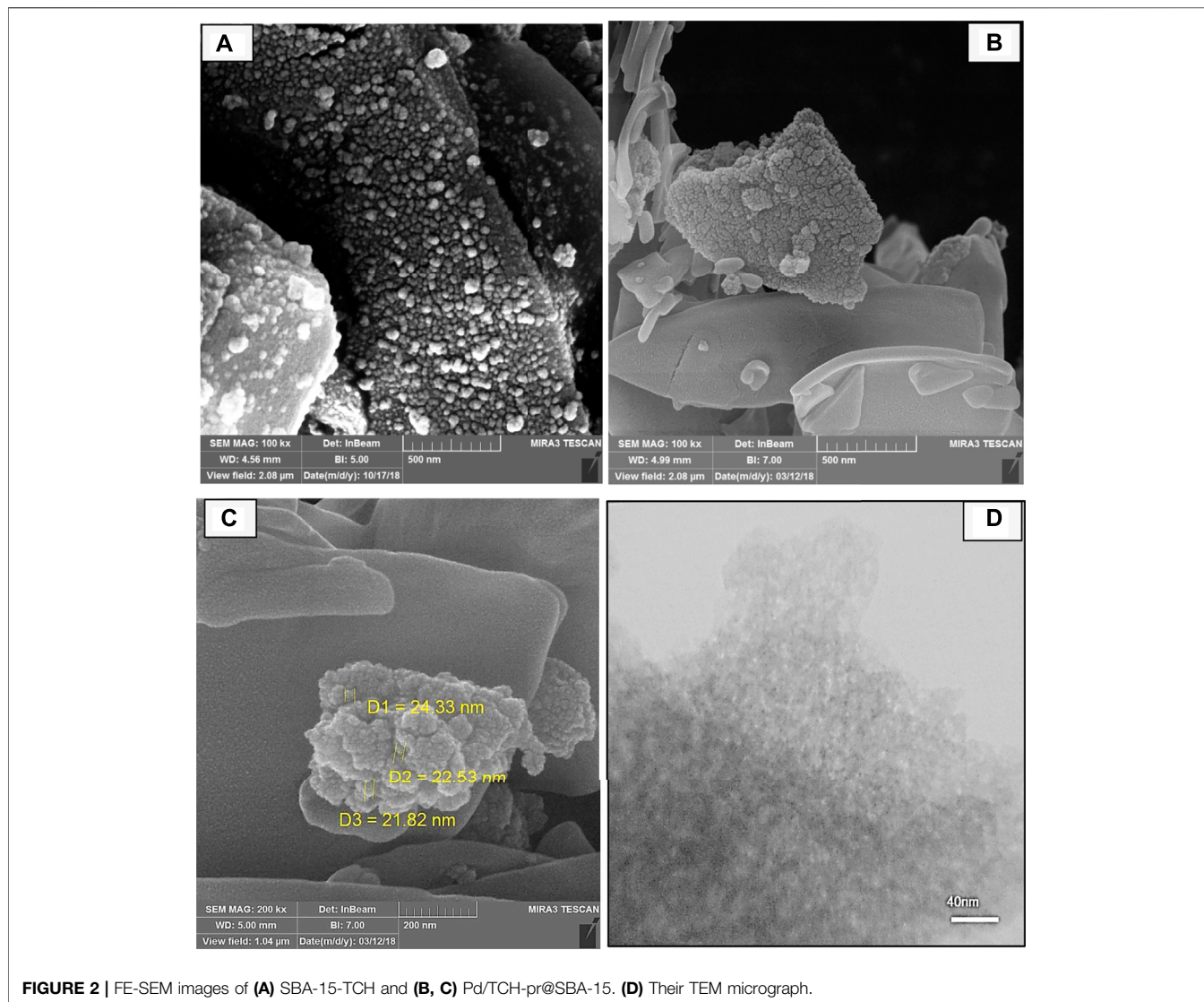
### Materials and Apparatuses

Chemical compounds were purchased from Sigma–Aldrich and Merck companies with a commercial grade and used as received without further purification. Melting points were determined in open capillaries using an electrothermal digital melting point

apparatus and were uncorrected. Fourier transform infrared (FT-IR) spectra were recorded on a JASCO 4200-A spectrometer with KBr pellets.  $^1\text{H}$ NMR and  $^{13}\text{C}$ NMR spectra were recorded on a Bruker spectrometer (300–500 MHz) using  $\text{DMSO-}d_6$  as a solvent and  $\text{Me}_4\text{Si}$  as an interior standard. The morphology of the functionalized SBA-15 was investigated using a Leica Cambridge S 360 scanning electron microscope (scanning electron microscopy (SEM) and field emission scanning electron microscopy (FE-SEM)). Transmission electron microscopy (TEM) images were recorded on a Philips CM10 microscope with an acceleration voltage of 100 kV.  $\text{N}_2$  adsorption–desorption isotherms of SBA-15 nanocomposites were measured at the temperature of liquid nitrogen using a Micromeritics system (made in the United States). The Brunauer–Emmett–Teller surface area of the nanoparticles was calculated using the BET method.

### The Typical Procedure for the Synthesis of Pd/TCH-pr@SBA-15 Nanocatalysts

Chloropropyl-functionalized SBA (Pr-Cl@SBA-15) was prepared according to the literature by Kalhor et al. (2019). Then, for the synthesis of TCH/Pr-Cl@SBA-15 nanohybrids, in a 100 ml round-bottom flask, 1.2 g (11.3 mmol) of TCH was dissolved in 18 ml of acetonitrile and stirred for 1 h. Next, 1.17 g (6.67 mmol) of KI and 1.2 g of SBA-15-Cl were added to the reaction mixture and refluxed for 15 h. The solvent was removed, and the mixture was collected using a centrifuge. The resultant solid mixture was stirred in 50 ml distilled water to remove the excipients or unreacted particles, separated by vacuum filtration



using a Buchner funnel, and dried in an oven at 50 °C for 12 h. For the complex formation of Pd(II) ions on functionalized SBA-15, 0.15 g (0.67 mmol) of palladium acetate was dissolved in 10 ml acetone, and 1.30 g of SBA-15-TCH was added to the solution and stirred at room temperature for 3 h. The mixture was filtered, washed with acetone and THF, and dried in an oven at 50 °C for 3 h to obtain the Pd/TCH-pr@SBA-15.

### General Procedure for the Preparation of 1,3-Thiazolidin-4-ones

A mixture of 2-aminobenzimidazole or 2-aminobenzothiazole (1 mmol), an aldehyde (1 mmol), thioglycolic acid (1 mmol), and 3 wt% of the Pd/TCH-pr@SBA-15 nanocatalyst (0.004 g) in 5 ml H<sub>2</sub>O/acetone (1:1) was stirred at room temperature. After completion of the organic reaction [thin layer chromatography monitoring using hexane and ethyl acetate (2:1) as eluents], the nanocatalyst was intercepted by filtration and the filtrate was

added to 10 ml of cold water. The precipitate was filtered out and washed with a cold ethanol–water mixture. Most of the desired products were obtained on a pure basis; however, for further purity, these can be recrystallized from the water–ethanol mixture. All the 1,3-thiazolidin-4-one products were known and identified by spectroscopic data and by comparing their melting points with literature values. Spectroscopic data for some 1,3-thiazolidin-4-ones are given in the following sections.

### Spectroscopic Data for the Selected Compounds

#### 3-(1*H*-Benzo[d]imidazol-2-yl)-2-(2-chlorophenyl)thiazolidin-4-one (4f)

FT-IR (KBr) ( $\nu_{\max}$ ): 3444, 3349 (NH), 2925 (C-H), 1683 (C=O), 1535 (C=N), 1447, 1303, 1269 (C=C), 1170 (C-N), 743, and 647 (C-S-C) cm<sup>-1</sup>; <sup>1</sup>H-NMR (500 MHz, DMSO-*d*<sub>6</sub>)  $\delta_{\text{H}}$ : 12.52 (1H, s, NH), 7.56 (2H, t,  $J = 7.60$  Hz, H-Ar), 7.39 (1H, d,  $J = 7.90$  Hz,

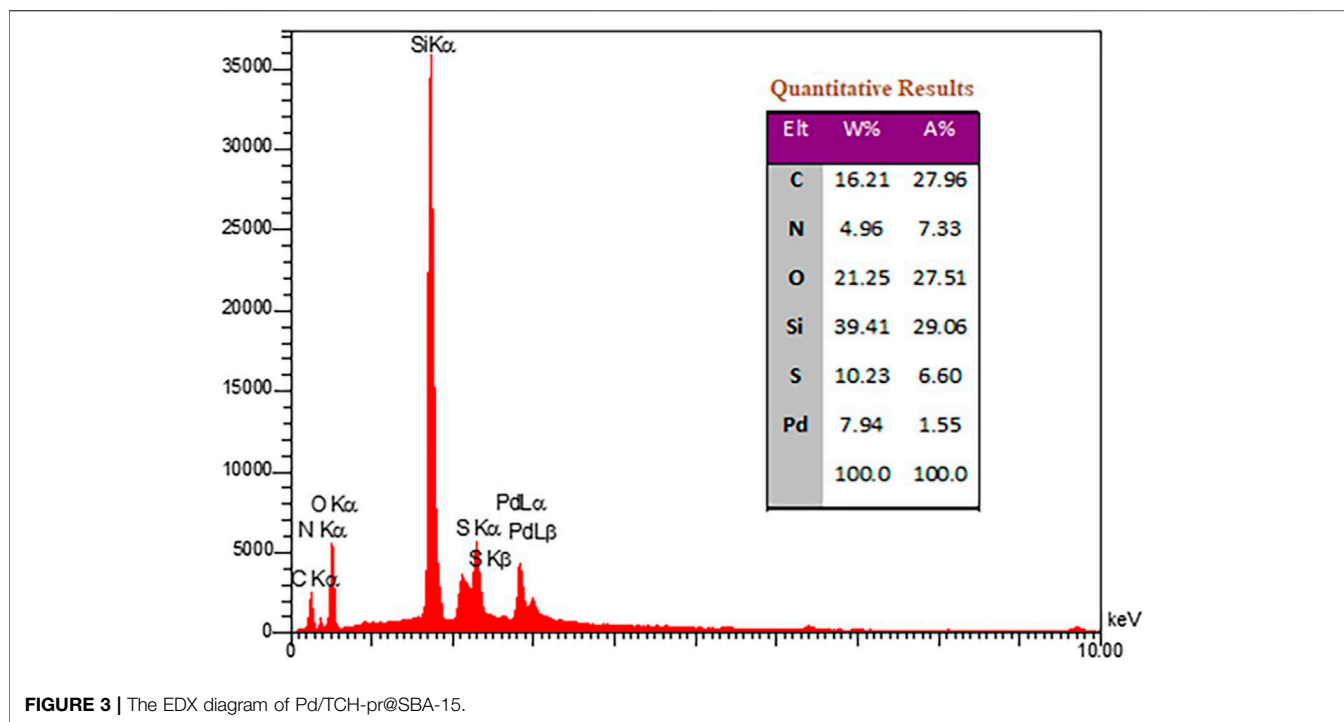


FIGURE 3 | The EDX diagram of Pd/TCH-pr@SBA-15.

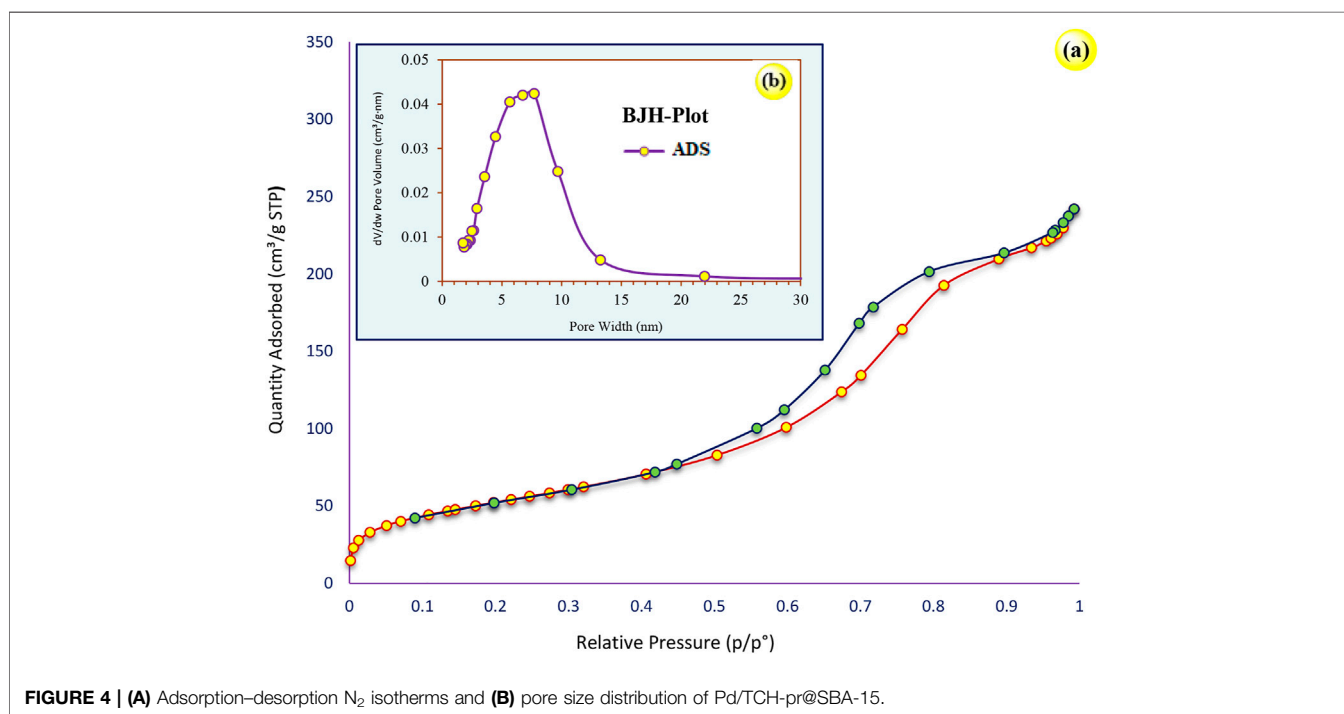


FIGURE 4 | (A) Adsorption-desorption  $N_2$  isotherms and (B) pore size distribution of Pd/TCH-pr@SBA-15.

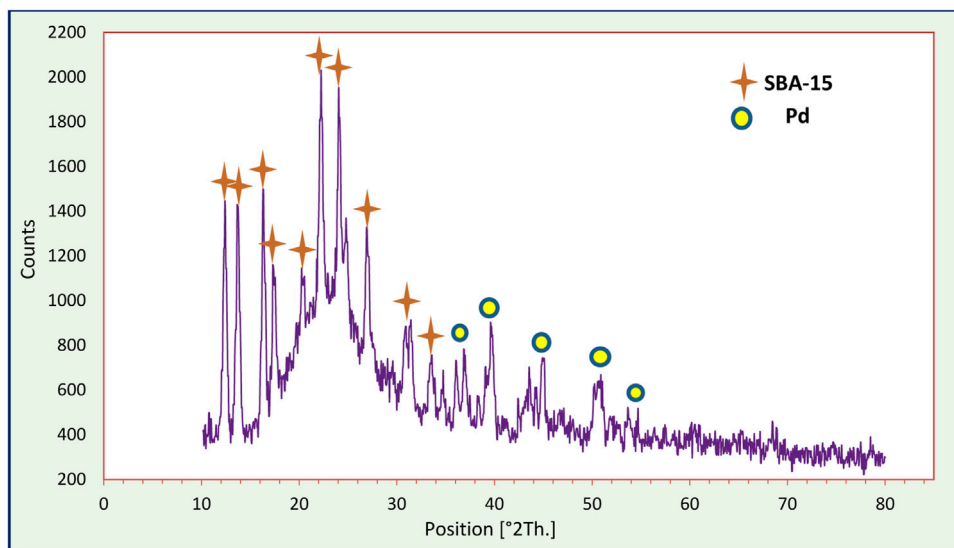
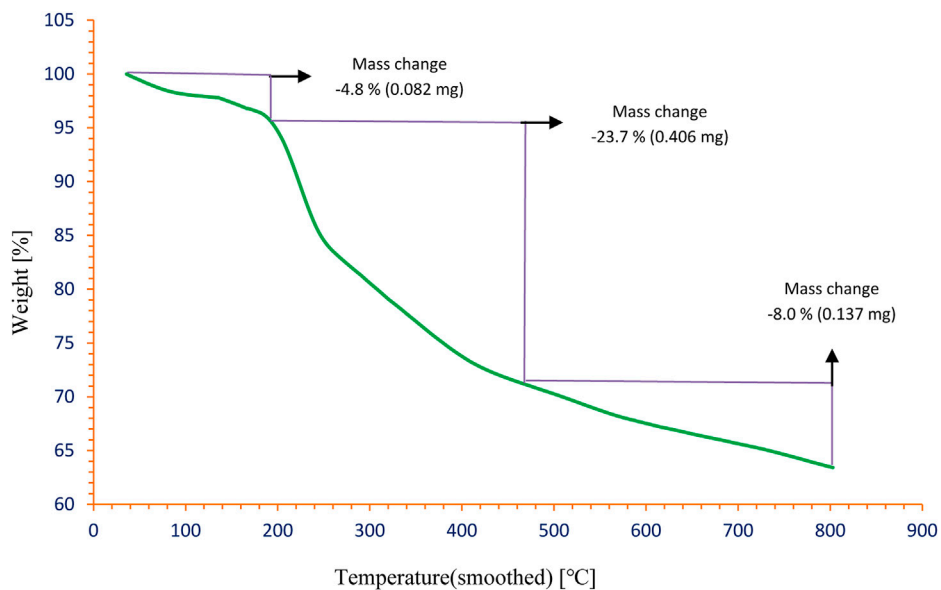
H-Ar), 7.33 (1H, t,  $J = 7.60$  Hz, H-Ar), 7.27 (1H, t,  $J = 7.55$  Hz, H-Ar), 7.14–7.07 (3H, m, H-Ar), 6.85 (1H, s, CH), 4.14 (1H, d,  $J = 16.45$  Hz, SCH-diastereotopic), and 4.01 (1H, d,  $J = 16.50$  Hz, SCH-diastereotopic) ppm;  $^{13}C$ -NMR (125 MHz, DMSO- $d_6$ )  $\delta_C$ : 172.2, 144.7, 140.2, 138.3, 133.3, 131.5, 130.5, 129.9, 128.1, 125.2, 122.2, 122.0, 118.2, 112.4, 59.5, and 32.1 ppm; MS ( $m/z$ , %): 329 ( $M^+$ , 10), 294 (100), and 220 (94).

### 3-(Benzo[d]thiazol-2-yl)-2-(4-bromophenyl)thiazolidin-4-one (4m)

FT-IR (KBr) ( $\nu_{max}$ ): 1690 (C=O), 1617, 1537 (C=N), 1467, 1369, 1274 (C=C), 1228 (C-N), and 658 (C-S-C)  $cm^{-1}$ ;  $^1H$ -NMR (300 MHz, DMSO- $d_6$ )  $\delta_H$ : 8.02 (1H, d,  $J = 7.74$  Hz, H-Ar), 7.66 (1H, d,  $J = 8.75$  Hz, H-Ar), 7.53 (2H, d,  $J = 8.41$  Hz, H-Ar), 7.41–7.30 (4H, m, H-Ar), 6.89 (1H, s, CH), 4.31 (1H,

**TABLE 1** | Structural and textural parameters of the SBA-15 and Pd/TCH@SBA-15 composites.

Sample	M <sup>a</sup> (%)	S <sub>BET</sub> <sup>b</sup> (m <sup>2</sup> .g <sup>-1</sup> )	V <sub>BJH</sub> <sup>c</sup> (cm <sup>3</sup> .g <sup>-1</sup> )	D <sub>BJH</sub> <sup>d</sup> (nm)	V <sub>HKM</sub> <sup>e</sup> (cm <sup>3</sup> .g <sup>-1</sup> )	P <sub>APS</sub> <sup>f</sup> (nm)
SBA-15	-	629.63	0.836	5.11	0.258	9.529
Pd/TCH-pr@SBA-15	22	184.33	0.382	7.09	0.077	31.482

<sup>a</sup>Initial percentage of copper ions.<sup>b</sup>Specific surface area.<sup>c</sup>Pore volume.<sup>d</sup>Pore size (calculated from the adsorption branch).<sup>e</sup>Maximum pore volume at  $p/p^* = 0.172869793$  (estimated using the Horvath-Kawazoe method).<sup>f</sup>Average nanoparticle size (estimated using the Temkin method).**FIGURE 5** | The XRD spectrum of the organometallic nanocatalyst Pd/TCH-pr@SBA-15.**FIGURE 6** | The TGA curve of Pd/TCH-pr@SBA-15.

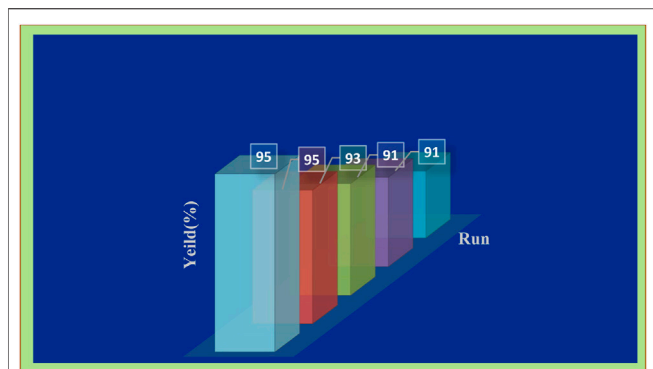


**FIGURE 7** | The study on the catalyst recycling activity in the synthesis of product **4c**.

d,  $J = 16.73$  Hz, SCH<sub>2</sub>), and 4.05 (1H, d,  $J = 16.76$  Hz, SCH<sub>2</sub>) ppm; <sup>13</sup>C-NMR (75 MHz, DMSO-*d*<sub>6</sub>) δ<sub>C</sub>: 31.8, 62.1, 121.0, 121.2, 121.9, 124.4, 126.3, 127.7, 131.2, 131.5, 140.6, 147.5, 155.9, and 171.6 ppm; MS (m/z, %): 392.4 (M<sup>+</sup>, 58.4), 350.4 (42.5), 317.4 (83.2), and 135.5 (100).

### 3-(Benzo[d]thiazol-2-yl)-2-(4-methoxyphenyl)thiazolidin-4-one (**4n**)

FT-IR (KBr) (ν<sub>max</sub>): 1690 (C=O), 1617, 1537 (C=N), 1467, 1369, 1274 (C=C), 1228 (C-N), and 658 (C-S-C) cm<sup>-1</sup>; <sup>1</sup>H-NMR

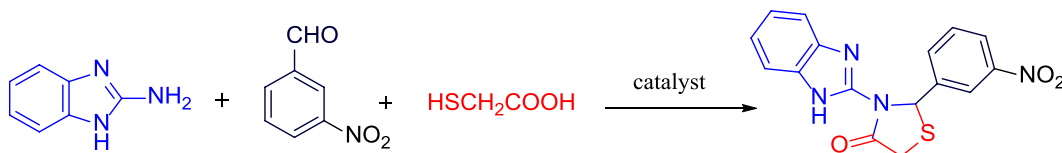
(300 MHz, DMSO-*d*<sub>6</sub>) δ<sub>H</sub>: : 8.02 (1H, d,  $J = 7.69$  Hz, H-Ar), 7.68 (1H, d,  $J = 7.97$  Hz, H-Ar), 7.42–7.29 (4H, m, H-Ar), 6.88 (2H, d,  $J = 7.51$  Hz, H-Ar), 6.85 (1H, s, CH), 4.31 (1H, d,  $J = 16.79$  Hz, SCH<sub>2</sub>), 4.04 (1H, d,  $J = 16.81$  Hz, SCH<sub>2</sub>), and 3.69 (3H, s, OMe) ppm; <sup>13</sup>C-NMR (75 MHz, DMSO-*d*<sub>6</sub>) δ<sub>C</sub>: 31.9, 55.0, 62.5, 113.9, 121.2, 121.8, 124.3, 126.3, 127.0, 131.2, 132.9, 147.6, 155.9, 158.9, and 171.6 ppm; MS (m/z, %): 342.6 (M<sup>+</sup>, 99.9), 300.6 (71.6), 267.6 (80.5), 208.5 (68.8), and 135.5 (100).

## RESULTS AND DISCUSSION

### Preparation and Characterization of the Pd/TCH-Pr@SBA-15 Nanocatalyst

The organometallic nanohybrid composite Pd/TCH-pr@SBA-15 was designed and fabricated according to **Scheme 2**. SBA-15 was functionalized with the organosilane precursor 3-chloropropyltriethoxysilane according to the reported method by Kalhor et al. (2019). Then, this chloropropyl-grafted SBA-15 was refluxed with a TCH ligand followed by complexation with Pd(OAc)<sub>2</sub> to afford the supported Pd catalyst on the SBA-15 nanoparticles. Since the investigation of the composition, structure, and morphology of nanocatalysts is an important parameter in the prediction of their catalytic behavior, the structure of the Pd/TCH-pr@SBA-15 nanocomposite was first studied using different techniques and is discussed in the following.

**TABLE 2** | Optimization of the reaction conditions for the synthesis of 3-(1H-benzo[d]imidazol-2-yl)-2-(3-nitrophenyl)thiazolidin-4-one for the model reaction.

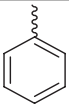
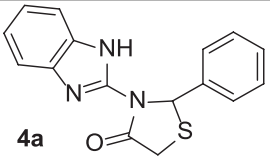
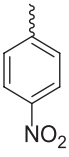
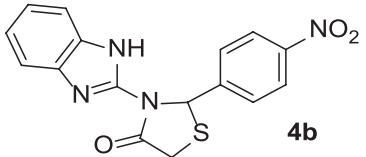
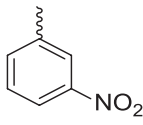
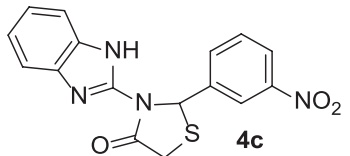
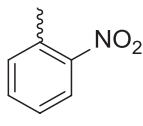
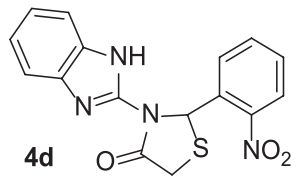
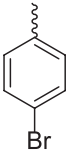
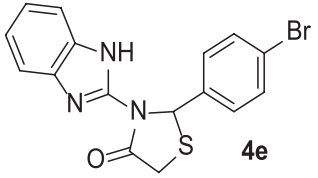
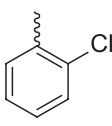
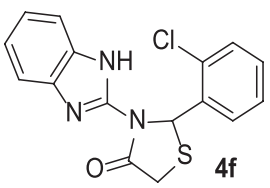
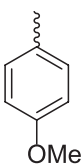
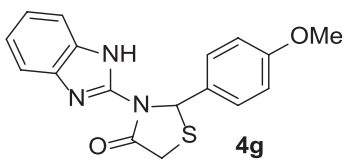
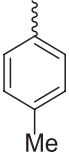
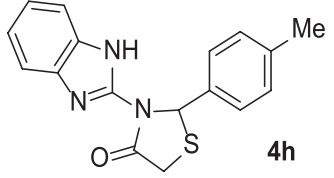
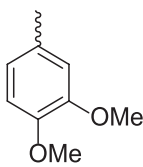
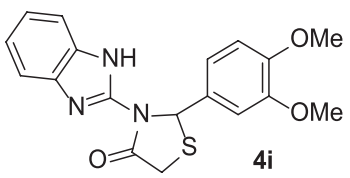


Entry	Catalyst loading (wt/wt%)	Solvent	Time (min)/temperature (°C)	Yield (%) <sup>a</sup>
1	5	EtOH	30/25	85
2	7	EtOH	25/25	77
3	3	EtOH	30/25	90
4	1.5	EtOH	45/25	67
5	3	EtOH/H <sub>2</sub> O (1:1)	45/25	72
6	3	Acetone	20/25	90
<b>7</b>	<b>3</b>	<b>Acetone/H<sub>2</sub>O (1:1)</b>	<b>20/25</b>	<b>95</b>
8	5	Acetone/H <sub>2</sub> O (1:1)	20/25	95
9	3	H <sub>2</sub> O	20/25	-
10	3	H <sub>2</sub> O	20/100	45
11	3	MeOH	20/25	73
12	3	CHCl <sub>3</sub>	20/25	trace
13	3	MeCN	20/25	67
14	3 (Pd(OAc) <sub>2</sub> )	Acetone/H <sub>2</sub> O (1:1)	20/25	55
15	3 (SBA-15)	Acetone/H <sub>2</sub> O (1:1)	20/25	trace
16	3 (TCH@SBA-15)	Acetone/H <sub>2</sub> O (1:1)	20/25	30
17	-	Acetone/H <sub>2</sub> O (1:1)	60/25	trace

*Bold values are for the optimal reaction conditions.*

<sup>a</sup>Isolated yield.

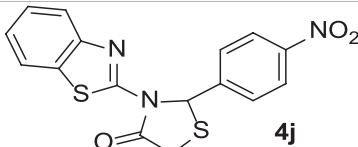
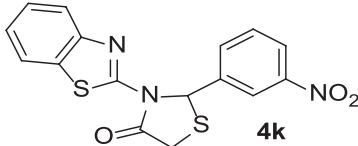
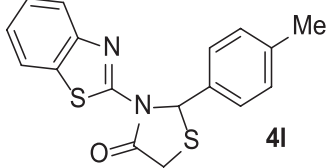
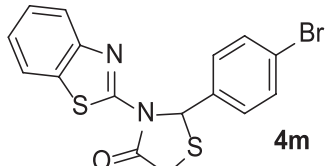
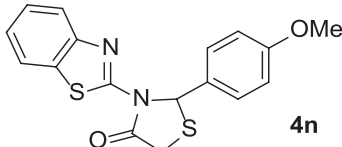
**TABLE 3** | Synthesis of products **4a–n** in the presence of 3 wt% of Pd/TCH-pr@SBA-15 and in an acetone/H<sub>2</sub>O mixture at room temperature.

Entry	Ar-CHO	Product	Time (min)	M.p. (°C)	Yield (%) <sup>a</sup>
1		 <b>4a</b>	22	208–210 (209–210) <sup>b</sup>	88
2		 <b>4b</b>	15	208–210 (208–210)	97
3		 <b>4c</b>	20	147 (147–148)	95
4		 <b>4d</b>	18	266–267 (265–267)	92
5		 <b>4e</b>	20	245 (244–246)	94
6		 <b>4f</b>	18	220–221 (221–223)	91
7		 <b>4g</b>	23	216–217 (216)	87
8		 <b>4h</b>	24	219 (220)	86
9		 <b>4i</b>	22	167–168 (167–169)	91

(Continued on following page)



**TABLE 3** | (Continued) Synthesis of products **4a–n** in the presence of 3 wt% of Pd/TCH-pr@SBA-15 and in an acetone/H<sub>2</sub>O mixture at room temperature.

Entry	Ar-CHO	Product	Time (min)	M.p. (°C)	Yield (%) <sup>a</sup>
10	<b>2b</b>	 <b>4j</b>	15	176–178 (176)	98
11	<b>2c</b>	 <b>4k</b>	18	170–171 (171–172)	96
12	<b>2h</b>	 <b>4l</b>	22	192 (194–195)	89
13	<b>2e</b>	 <b>4m</b>	19	163–164 (161–162)	95
14	<b>2g</b>	 <b>4n</b>	21	176 (177–178)	92

The bold values are for the aldehyde derivatives code.

<sup>a</sup>Isolated yield.

<sup>b</sup>Melting points in parentheses are reported in the literature by Kalhor and Banibairami (2020).

In order to show the nanostructure functional groups, the crude SBA-15 FT-IR spectra and its modified spectra were analyzed. **Figure 1A** demonstrates the spectrum of SBA-15 nanoparticles. The broad absorption band appearing at  $3431\text{ cm}^{-1}$  is due to the stretching vibration of Si-OH functional groups. Also, absorption bands at  $1631$  and  $1097\text{ cm}^{-1}$  are specification of water bonded to the silica backbone and asymmetric stretching of Si-O-Si, respectively (Safaei-Ghomi et al., 2016). The appearance of signals in the  $3273$  and  $3205\text{ cm}^{-1}$  regions (NHNH<sub>2</sub> group) in **Figure 1B** confirms the presence of thiocarbonyl group in the nanostructure. The stretching vibrations C=S are characterized by two index wavenumbers ( $1290$  and  $931\text{ cm}^{-1}$ ) in TCH, respectively. The peak in the  $2954\text{ cm}^{-1}$  region indicates the binding of CH<sub>2</sub> groups to the silicate nanostructure. From the comparison of the last two spectra, given the identical chemical nature of the two compounds, the apparent similarity of the

spectra is natural and predictable. However, in the spectrum of the organometallic nanostructure, changes in wavenumbers of amine (NH<sub>2</sub>) and thione (C=S) functional groups can be observed, which is related to the coordination interactions of Pd(II) ions with nitrogen and sulfur atoms in the TCH section (Burns, 1968; Braibanti et al., 1969; Alizadeh et al., 2013). Overall, the comparison of the infrared spectra, as expected, confirms the immobilization of the desired organometallic functional groups on the surface of SBA-15.

FE-SEM was used to investigate the surface morphology of SBA-15-TCH and Pd/TCH@SBA-15 composite nanomaterials, and the corresponding images are shown in **Figure 2**. As observed, SBA-15-TCH has a crystalline structure in the form of a spherical shape (**Figure 2A**). Furthermore, the structure of the Pd/TCH@SBA-15 nanocomposite is clearly demonstrated in **Figures 2B,C**. The original structure of SBA-15 remained unchanged following functionalization. According to

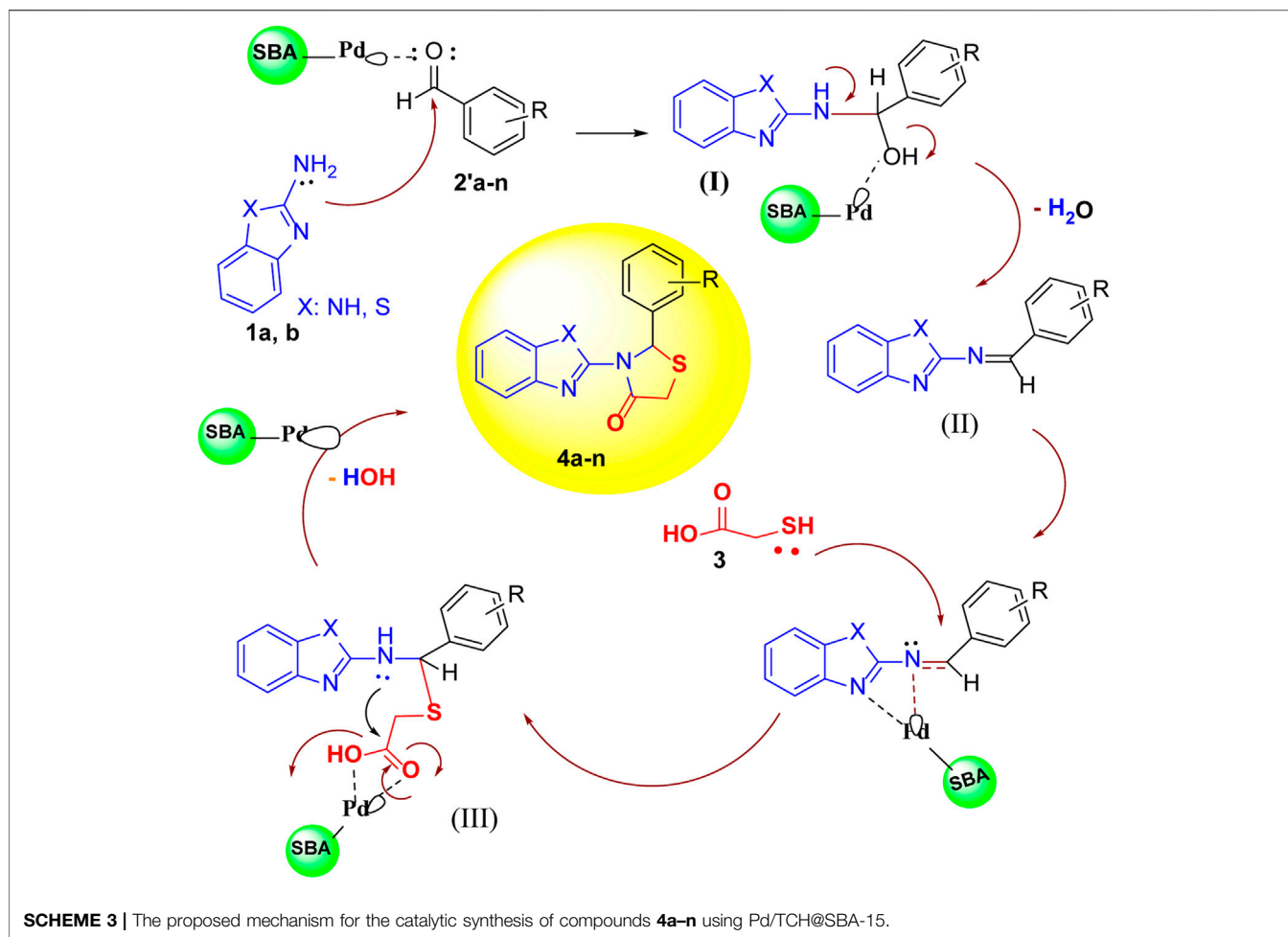


**Figure 2C**, the particle size is in the range of 21–24 nm. The TEM micrographs in **Figure 2C** illustrate regular mesoporous channels of silica after modification.

The energy-dispersive X-ray spectroscopy (EDX) of the prepared organometallic nanosystem is presented in **Figure 3**. The signals corresponding to C, N, S, O, Si, and Pd elements as well as the quantitative results of EDX confirm the presence of Pd(II) and propyl-TCH moieties in the Pd/TCH-pr@SBA-15 nanostructure. Moreover, the Pd content of the Pd/TCH-pr@SBA-15 estimated by atomic absorption spectroscopy is 22% wt/wt%.

**Figure 4A** shows the  $N_2$  adsorption–desorption isotherms of Pd/TCH-pr@SBA-15 nanocomposites. As observed, this structure shows type I isotherm, representing microporous and mesoporous frameworks. According to **Figure 4B**, the  $N_2$  adsorption–desorption diagram of Pd/TCH-pr@SBA-15 shows type IV isotherms with a sharp capillary condensation step at high relative pressure and an H1 hysteresis loop in the 0.4–0.9  $p/p^0$  range, which reveals the presence of large channel-like pore structures in a narrow range of size, based on the IUPAC classification (Safaei-Ghomi and Bakhtiari, 2018). Also, by the shape of its hysteresis, it can be seen that Pd/TCH-pr@SBA-15 has cylindrical pores and the initial nanostructure after

functionalization is still retained (Sánchez-Velandia and Villa, 2019).

Moreover, the BJH pore size distribution diagram in **Figure 4B** shows that the major width of the cavities is in the range of 2–21 nm and cavities are microporous and mesoporous (Sarkar et al., 2009).

The structural data of the SBA-15 and Pd/TCH-pr@SBA-15 nanoparticles are listed in **Table 1**. The BET surface area and pore volume of Pd/TCH@SBA-15 decrease owing to the functionalization steps of SBA-15 which may be due to the significant loading of the complex into the mesoporous channels of SBA-15 (Alizadeh et al., 2013). In addition, the average nanoparticle size is increased to 33 nm compared to that of SBA-15 (9 nm), which can confirm the grafting of organometallic functional groups on the substrate surface and the occupation of cavities.

The X-ray diffraction (XRD) pattern of Pd/TCH-pr@SBA-15 is shown in **Figure 5**. The XRD pattern of SBA-15 matches with the standard XRD data (JCDPS card no. 01-086-1561), in which the appearance of sharp diffraction peaks in it indicates a crystalline structure. The flattening of the peak at angles of 20°–25° ( $2\theta$ ) is due to the presence of amorphous silica phase in the SBA-15 structure, which corresponds to the mentioned

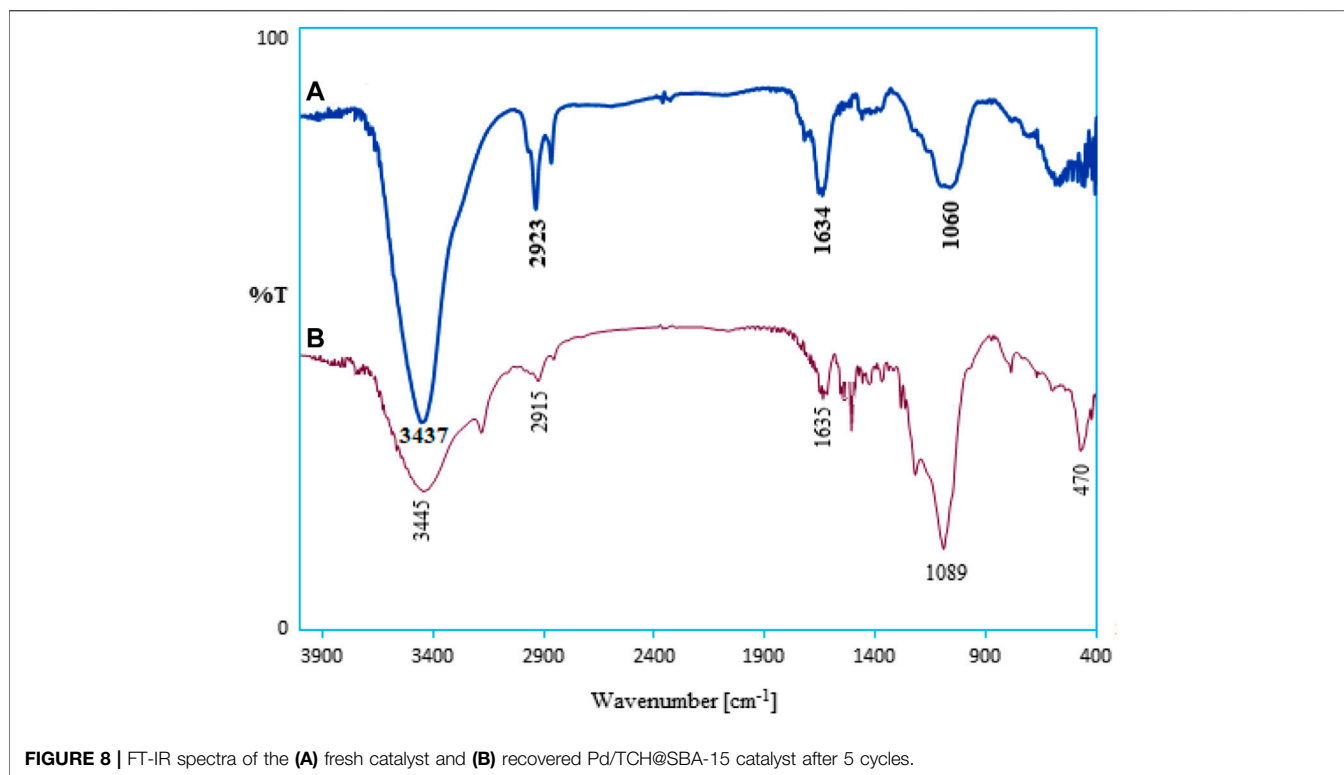


**TABLE 4** | Comparison of the activity of various catalysts for the synthesis of 1,3-thiazolidin-4-ones.

Entry	Catalyst	Condition	Time (min)	Yield (%) (ref.)
1	DCC (60 mol%)	THF, RT	60	59–95 (Srivastava et al. (2001))
2	Pd NPs (10 mol%)	Solvent-free, 100 °C	60	71–90 (Harale et al. (2016))
3	Ni@zeolite-Y (10 wt%)	EtOH, RT	25–35	80–95 (Kalhor et al. (2018))
4	HClO <sub>4</sub> -SiO <sub>2</sub> (47 wt%)	PhCH <sub>3</sub> , 100 °C	180–360	70–88 (Kumar et al. (2013))
5	Alum (10 mol%)	M. V. grind, RT	25–30	85–93 (Jadhav et al. (2015))
6	Silica gel (0.5 g)	THF, RT	240–420	77–96 (Thakare et al. (2014))
7	DIPEA (3 equiv)	PhCH <sub>3</sub> , reflux	180–240	65–85 (Chate et al. (2016))
8	CoFe <sub>2</sub> O <sub>4</sub> @SiO <sub>2</sub> /Pr-NH <sub>2</sub> (0.7 mol%)	PhCH <sub>3</sub> , reflux	120–480	75–85 (Safaei-Ghomi et al. (2016))
9	Ni/SO <sub>3</sub> H@zeolite-Y (5 wt%)	H <sub>2</sub> O-acetone, RT	15–25	85–97 (Kalhor and Banibairami (2020))
10	Fe <sub>3</sub> O <sub>4</sub> @SiO <sub>2</sub> /APTOSS (8 wt%)	Solvent-free, 60 °C	30	90–94 (Safaei-Ghomi et al. (2016))
11	La(NO <sub>3</sub> ) <sub>3</sub> (10 mol%)	EtOH, RT	24	77–90 (Kalhor et al. (2017))
12	MCM-41@Si-L, CuSO <sub>4</sub> (7 wt%)	PhCH <sub>3</sub> , 110 °C	720	77–99 (Pang et al. (2016))
13	Catalyst-free	H <sub>2</sub> O, RT	240–420	79–96 (Thakare et al. (2016))
14	Pd@SBA-15 (3 wt%)	H <sub>2</sub> O-acetone, RT	15–24	87–97 (this work)

JCPDS card number. The main peaks at  $2\theta$  values of  $39.9^\circ$  and  $45.6^\circ$  belong to crystal indexes of (111) and (200), respectively, which indicates the presence of palladium in the nanocomposite (Duan et al., 2017; Ulusal and Güzel, 2018). Also, the weak peaks at  $2\theta = 36.1^\circ$ ,  $50.7^\circ$ , and  $54.7^\circ$  related to crystal indexes of (101), (202), and (112), respectively, according to the standard XRD data (JCPDS card no. 43-1024), can indicate the presence of Pd<sup>2+</sup> ions in the structure (Ganji et al., 2013; Payehghadr et al., 2019). The observation of these points indicates that the existence of an ordered two-dimensional (2D) hexagonal structure and also the framework of SBA-15 were not damaged after modification. The

size of the Pd-TCH@SBA-15 nanostructure crystal determined from the XRD pattern using the Debye-Scherrer equation was 27.16 nm.

**Figure 6** shows the thermogravimetric analysis (TGA) curve of Pd/TCH-pr@SBA-15. As observed in the TGA curve, the weight loss of 4.8% (0.082 mg) in the first step in the temperature range of 50–190°C is due to physical and chemical desorption of water molecules. The second weight loss of 23.7% (0.406 mg) observed in the temperature range of 190–450°C is associated with the degradation of organic and complex (TCH-Pd) species. Thus, the SBA-15 surface is

functionalized by organic groups. The final weight loss of 8.0% (0.137 mg) in the temperature range of 450–800°C may be due to the change in the silica structure (Liu et al., 2010).

## Catalytic Activities of Pd/TCH@SBA-15 in the Solvent-Free Synthesis of 3-Benzimidazolyl- or Benzothiazoleyl-1,3-thiazolidin-4-ones

In the preliminary experiment to find optimal conditions for the synthesis of 2-aryl-3-benzimidazolyl or benzthiazoleyl-1,3-thiazolidin-4-ones, we used 3-nitrobenzaldehyde, 2-aminobenzimidazole, and thioglycolic acid as starting materials in the presence of Pd/TCH-pr@SBA-15 as a new nanocatalyst for a model reaction. To achieve optimal conditions, the desired reaction was carried out with different solvents and catalyst amounts as a green process. It is shown in **Table 2** that when 3 wt% of Pd/TCH-pr@SBA-15 was used, 95% of the desired product was formed at 25 °C in acetone/H<sub>2</sub>O (1:1) (**Table 2**, entry 7). Moreover, it was observed that this organic reaction did not improve in the presence of Pd(OAc)<sub>2</sub>, SBA-15, and TCH@SBA-15 (**Table 2**, entries 14–16, respectively). Also, a glancing look at **Table 2** exhibits that the reaction yields increase in the aprotic–protic polar solvent mixture (water/acetone). On the contrary, without the nanocatalyst, the reaction did not proceed (**Table 2**, entry 17).

Under the optimized conditions of the model reaction, a study on a variety of aldehyde derivatives was carried out, and the representative results are presented in **Table 3**. Different aryl aldehydes were transformed into corresponding 3-benzimidazolyl or benzthiazoleyl-1,3-thiazolidin-4-ones, with good to excellent yields.

A proposed mechanism for the catalytic synthesis of 1,3-thiazolidin-4-ones by Pd-SBA-15 is shown in **Scheme 3**. First, the Pd/TCH-pr@SBA-15 nanocatalyst as a Lewis acid activates the carbonyl groups of aldehyde (**2a–n**). Then, the NH<sub>2</sub> group of 2-aminobenzimidazole (or 2-aminobenzothiazole) as a nucleophile attacks the activated carbonyl to afford the intermediate **I** that is followed by the catalytic oxidation process and removal of a H<sub>2</sub>O molecule to form intermediate **II**. The Schiff base **II** is a stable structure and can be separated from the reaction moiety. In the second catalytic activation stage, the nucleophilic attack of the thiol group of thioglycolic acid to imine takes place to form the intermediate **III**. Finally, after intermolecular nucleophilic attack and loss of the second water molecule, cyclization of the 1,3-thiazolidin-4-one products **4a–n** can be performed.

The reusability of the heterogeneous catalyst was investigated for a model reaction under optimized conditions. After completion of the catalytic process, the Pd/TCH-pr@SBA-15 composite was easily separated by simple filtration from the reaction mixture. It was washed with ethanol several times, dried in an oven at 70 °C for 60 min, and then reused in the next reaction. The results of recyclability of the Pd/TCH-pr@SBA-15 composite are shown in **Figure 7**. No significant reduction in the catalyst activity was observed after five times. Therefore, the doped -(CH<sub>2</sub>)<sub>3</sub>-TCH-Pd composite on SBA-15 as an applicable support is found to be a superior efficient catalytic organometallic nanosystem for this reaction.

The basic structure of the recycled catalyst was also affirmed with FT-IR spectra, and there was no difference in the FT-IR spectra of the fresh and recovered catalysts, approximately (**Figure 8**).

Also, the Pd content in the nanocatalyst after the fifth reaction cycle was marginally decreased to 21.7% wt/wt (this reduction can be due to the error in experimental chemical analysis). As a result, the heterogeneous nature of the nanocatalyst is confirmed in this reaction and no palladium leaching occurred.

A comparison of the catalytic activity of the Pd/TCH-pr@SBA-15 nanocomposite and other reported various catalysts for the synthesis of 1,3-thiazolidin-4-ones is listed in **Table 4**. A comparative look at **Table 4** reveals that the nanocatalyst performance is better than that of other reported catalysts in terms of yield, amount of the catalyst, and reaction time.

## CONCLUSION

In this study, the SBA-15-supported TCH-palladium complex was successfully designed and characterized as a novel organometallic nanocatalyst for the three-component synthesis of 3-benzimidazolyl or benzothiazoleyl-1,3-thiazolidin-4-ones under green conditions. Some of the advantages of the present procedure include high product yields, short reaction time, easy purification process, application of nanotechnology in the catalytic process, recyclability, low cost, and nontoxicity of the catalyst. These benefits make the procedure more environmentally benign and a significant contribution towards green chemistry.

## DATA AVAILABILITY STATEMENT

The original contributions presented in the study are included in the article/**Supplementary Material**; further inquiries can be directed to the corresponding author.

## AUTHOR CONTRIBUTIONS

All authors listed have made a substantial, direct, and intellectual contribution to the work and approved it for publication.

## ACKNOWLEDGMENTS

The authors gratefully acknowledge the financial support from the Payame Noor University for this work.

## SUPPLEMENTARY MATERIAL

The Supplementary Material for this article can be found online at: <https://www.frontiersin.org/articles/10.3389/fchem.2021.723207/full#supplementary-material>

## REFERENCES

- Alizadeh, A., Khodaei, M. M., Kordestania, D., and Beygzadeh, M. (2013). A biguanide/Pd-Decorated SBA-15 Hybrid Nanocomposite: Synthesis, Characterization and Catalytic Application. *J. Mol. Catal. A: Chem.* 372, 167–174. doi:10.1016/j.molcata.2013.02.027
- Bhuyan, D., Saikia, M., and Saikia, L. (2015). Magnetically Recoverable Fe<sub>3</sub>O<sub>4</sub>@SBA-15: An Improved Catalyst for Three Component Coupling Reaction of Aldehyde, Amine and Alkyne. *Catal. Commun.* 58, 158–163. doi:10.1016/j.catcom.2014.09.011
- Biffis, A., Centomo, P., Del Zotto, A., and Zecca, M. (2018). Pd Metal Catalysts for Cross-Couplings and Related Reactions in the 21st Century: A Critical Review. *Chem. Rev.* 118, 2249–2295. doi:10.1021/acs.chemrev.7b00443
- Braibanti, A., Dallavalle, F., and Leporati, E. (1969). Complexes of Thiocarbonylhydrazide with Divalent Metals: Stability Constants in Aqueous Solutions. *Inorg. Chim. Acta* 3, 459–462. doi:10.1016/S0020-1693(00)92533-7
- Burns, G. R. (1968). Metal Complexes of Thiocarbonylhydrazide. *Inorg. Chem.* 7, 277–283. doi:10.1021/ic50060a022
- Calò, V., Nacci, A., Monopoli, A., and Montingelli, F. (2005). Pd Nanoparticles as Efficient Catalysts for Suzuki and Stille Coupling Reactions of Aryl Halides in Ionic Liquids. *J. Org. Chem.* 70, 6040–6044. doi:10.1021/jo5050801q
- Chate, A. V., Tathe, A. G., Nagtilak, P. J., Sangle, S. M., and Gill, C. H. (2016). Efficient Approach to Thiazolidinones via a One-Pot Three-Component Reaction Involving 2-Amino-1-Phenylethanone Hydrochloride, Aldehyde and Mercaptoacetic Acid. *Chin. J. Catal.* 37, 1997–2002. doi:10.1016/S1872-2067(16)62536-6
- Cunico, W., Gomes, C., and Vellaco Jr., W. (2008). Chemistry and Biological Activities of 1,3-Thiazolidin-4-Ones. *Mroc* 5, 336–344. doi:10.2174/157019308786242232
- Duan, Y., Zheng, M., Li, D., Deng, D., Wu, C., and Yang, Y. (2017). Synthesis of Pd/SBA-15 Catalyst Employing Surface-Bonded Vinyl as a Reductant and its Application in the Hydrogenation of Nitroarenes. *RSC Adv.* 7 (6), 3443–3449. doi:10.1039/C6RA26811K
- Feng, X., Yan, M., Zhang, T., Liu, Y., and Bao, M. (2010). Preparation And Application Of SBA-15 Supported Palladium Catalyst For Suzuki Reaction In Supercritical Carbon Dioxide. *Green Chem.* 12, 1758–1766. doi:10.1039/C004250A
- Fulvio, P. F., Pikus, S., and Jaroniec, M. (2005). Tailoring Properties of SBA-15 Materials by Controlling Conditions of Hydrothermal Synthesis. *J. Mater. Chem.* 15, 5049–5053. doi:10.1039/B511346F
- Ganji, S., Bukya, P., Vakati, V., Rao, K. S. R., and Burri, D. R. (2013). Highly Efficient and Expeditious PdO/SBA-15 Catalysts for Allylic Oxidation of Cyclohexene to Cyclohexenone. *Catal. Sci. Technol.* 3, 409–414. doi:10.1039/C2CY20627G
- Harale, R. R., Shitre, P. V., Sathe, B. R., and Shingare, M. S. (2016). Pd Nanoparticles: an Efficient Catalyst for the Solvent-free Synthesis of 2,3-Disubstituted-4-Thiazolidinones. *Res. Chem. Intermed.* 42, 6695–6703. doi:10.1007/s11164-016-2490-2
- Jadhav, S. A., Shioorkar, M. G., Chavan, O. S., Jadhav, S., Shioorkar, M., et al. (2015). An Alum Catalyzed Solvent-free One-Pot Multicomponent Synthesis of 4-thiazolidinone Derivatives. *Heterocyclic Lett.* 5, 375–382. Available at: <https://heteroletters.org/issue35/Paper-7.pdf>.
- Jain, A. K., Vaidya, A., Ravichandran, V., Kashaw, S. K., and Agrawal, R. K. (2012). Recent Developments and Biological Activities of Thiazolidinone Derivatives: a Review. *Bioorg. Med. Chem.* 20, 3378–3395. doi:10.1016/j.bmc.2012.03.069
- Kalhor, M., and Banibairami, S. (2020). Design of a New Multi-Functional Catalytic System Ni/SO<sub>3</sub>H@zeolite-Y for Three-Component Synthesis of N-Benzo-Imidazo- or -Thiazole-1,3-Thiazolidinones. *RSC Adv.* 10, 41410–41423. doi:10.1039/D0RA08237F
- Kalhor, M., Banibairami, S., and Mirshokraie, S. A. (2017). A One-Pot Multi-Component Reaction for the Facile Synthesis of Some Novel 2-aryl Thiazolidinones Bearing Benzimidazole Moiety Using La(NO<sub>3</sub>)<sub>3</sub>·6H<sub>2</sub>O as an Efficient Catalyst. *Res. Chem. Intermed.* 43, 5985–5994. doi:10.1007/s11164-017-2974-8
- Kalhor, M., Banibairami, S., and Mirshokraie, S. A. (2018). Ni@zeolite-Y Nanoporous; a Valuable and Efficient Nanocatalyst for the Synthesis of N-Benzimidazole-1,3-Thiazolidinones. *Green. Chem. Lett. Rev.* 11, 334–344. doi:10.1080/17518253.2018.1499968
- Kalhor, M., Rezaee-Baroonaghi, F., Dadras, A., and Zarnegar, Z. (2019). Synthesis of New TCH/Ni-based Nanocomposite Supported on SBA-15 and its Catalytic Application for Preparation of Benzimidazole and Perimidine Derivatives. *Appl. Organometal. Chem.* 33, e4784. doi:10.1002/aoc.4784
- Kalhor, M., Sajjadi, S. M., and Dadras, A. (2020). Cu/TCH-pr@SBA-15 Nanocomposite: a New Organometallic Catalyst for Facile Three-Component Synthesis of 4-Arylidene-Isoxazolidinones. *RSC Adv.* 10, 27439–27446. doi:10.1039/D0RA01314E
- Karimi, B., Abedi, S., Clark, J. H., and Budarin, V. (2006). Highly Efficient Aerobic Oxidation of Alcohols Using a Recoverable Catalyst: The Role of Mesoporous Channels of SBA-15 in Stabilizing Palladium Nanoparticles. *Angew. Chem.* 118, 4894–4897. doi:10.1002/ange.200504359
- Kim, J.-H., Park, J.-S., Chung, H.-W., Boote, B. W., and Lee, T. R. (2012). Palladium Nanoshells Coated with Self-Assembled Monolayers and Their Catalytic Properties. *RSC Adv.* 2, 3968–3977. doi:10.1039/C2RA00883A
- Kumar, D., Sonawane, M., Pujala, B., Jain, V. K., Bhagat, S., and Chakraborti, A. K. (2013). Supported Protic Acid-Catalyzed Synthesis of 2,3-disubstituted Thiazolidin-4-Ones: Enhancement of the Catalytic Potential of Protic Acid by Adsorption on Solid Supports. *Green. Chem.* 15, 2872–2884. doi:10.1039/C3GC41218K
- Lamblin, M., Nassar-Hardy, L., Hierso, J.-C., Fouquet, E., and Felpin, F.-X. (2010). Recyclable Heterogeneous Palladium Catalysts in Pure Water: Sustainable Developments in Suzuki, Heck, Sonogashira and Tsuji–Trost Reactions. *Adv. Synth. Catal.* 352, 33–79. doi:10.1002/adsc.200900765
- Liu, C., Tan, R., Yu, N., and Yin, D. (2010). Pt–Pd Bi-metal Nanoparticles Captured and Stabilized by Imine Groups in a Periodic Mesoporous Organosilica of SBA-15 for Hydrogenation of Nitrobenzene. *Micropor. Mesopor. Mat.* 131, 162–169. doi:10.1016/j.micromeso.2009.12.016
- Mobinikhaledi, A., Foroughifar, N., Kalhor, M., and Mirabolfathy, M. (2010). Synthesis and Antifungal Activity of Novel 2-benzimidazolylimino-5-arylidene-4-thiazolidinones. *J. Heterocycl. Chem.* 47, 77–80. doi:10.1002/jhet.264
- Molnár, Á. (2011). Efficient, Selective, and Recyclable Palladium Catalysts in Carbon–carbon Coupling Reactions. *Chem. Rev.* 111, 2251–2320. doi:10.1021/cr100355b
- Muñoz-Batista, M. J., Rodríguez-Pradon, D., Puente-Santiago, A. R., and Luque, R. (2018). Mechanochemistry: toward Sustainable Design of Advanced Nanomaterials for Electrochemical Energy Storage and Catalytic Applications. *ACS Sust. Chem. Eng.* 6, 9530–9544. doi:10.1021/acscuschemeng.8b01716
- Ostovar, S., Franco, A., Puente-Santiago, A. R., Pinilla-de Dios, M., Rodríguez-Pradón, D., Shaterian, H. R., et al. (2018). Efficient Mechanochemical Bifunctional Nanocatalysts for the Conversion of Isoeugenol to Vanillin. *Front. Chem.* 6, 77. doi:10.3389/fchem.2018.00077
- Pang, H. X., Hui, Y. H., Fan, K., Xing, X. J., Wu, Y., Yang, J. H., et al. (2016). Catalysis Study of Mesoporous MCM-41 Supported Schiff Base and CuSO<sub>4</sub>·5H<sub>2</sub>O in a Highly Regioselective Synthesis of 4-thiazolidinone Derivatives from Cyclocondensation of Mercaptoacetic Acid. *Chin. Chem. Lett.* 27, 335–339. doi:10.1016/j.ccl.2015.10.029
- Payehghadr, M., Qezelje-Haghighoo, H., Nourifard, F., Attaran, A., and Kalhor, M. (2019). Preconcentration of Ultra-traces of Cu (II) in Water Samples Using SBA-15 Sorbent Modified with a Thiocarbonylhydrazide Ligand Prior to Determination by Flame Atomic Absorption Spectrometry. *J. Serb. Chem. Soc.* 84 (5), 489–501. doi:10.2298/JSC180606093P
- Rajabi, F., Abdollahi, M., Diarjani, E. S., Osmolowsky, M. G., Osmolovskaya, O. M., Gómez-López, P., et al. (2019). Solvent-free Preparation of 1,8-Dioxo-Octahydroxanthenes Employing Iron Oxide Nanomaterials. *Materials* 12 (15), 2386. doi:10.3390/ma12152386
- Rodríguez-Pradón, D., Puente-Santiago, A. R., Balu, A. M., Muñoz-Batista, M. J., and Luque, R. (2019). Continuous Flow Synthesis of High Valuable N-Heterocycles via Catalytic Conversion of Levulinic Acid. *Front. Chem.* 7, 103. doi:10.3389/fchem.2019.00103
- Rodríguez-Pradón, D., Puente-Santiago, A. R., Balu, A. M., Muñoz-Batista, M. J., and Luque, R. (2019). Environmental Catalysis: Present and Future. *ChemCatChem.* 11, 18–35. doi:10.1002/cctc.201801248

- Safaei-Ghomi, J., and Bakhtiari, A. (2018). Ultrasonic Accelerated biginelli-Like Reaction by the Covalently Anchored Copper-isatoic Anhydride over the Modified Surface of Mesoporous SBA-15 to the Synthesis of Pyrimidines. *Chem. Select.* 3, 12704–12711. doi:10.1002/slct.201802435
- Safaei-Ghomi, J., Navvab, M., and Shahbazi-Alavi, H. (2016). CoFe<sub>2</sub>O<sub>4</sub>@SiO<sub>2</sub>/PrNH<sub>2</sub> Nanoparticles as Highly Efficient and Magnetically Recoverable Catalyst for the Synthesis of 1,3-Thiazolidin-4-Ones. *J. Sulfur. Chem.* 37, 601–612. doi:10.1080/17415993.2016.1169533
- Safaei-Ghomi, J., Nazemzadeh, S. H., and Shahbazi-Alavi, H. (2016). Preparation and Characterization of Fe<sub>3</sub>O<sub>4</sub>@SiO<sub>2</sub>/APTPOSS Core-Shell Composite Nanomagnetics as a Novel Family of Reusable Catalysts and Their Application in the One-pot Synthesis of 1,3-thiazolidin-4-one Derivatives. *Appl. Organometal. Chem.* 30, 911. doi:10.1002/aoc.3520
- Sánchez-Velandia, J. E., and Villa, A. L. (2019). Isomerization of  $\alpha$ - and  $\beta$ -pinene Epoxides over Fe or Cu Supported MCM-41 and SBA-15 Materials. *Appl. Catal. A: Gen.* 580, 17–27. doi:10.1016/j.apcata.2019.04.029
- Sarkar, K., Dhara, K., Nandi, M., Roy, P., Bhaumik, A., and Banerjee, P. (2009). Selective Zinc(II)-Ion Fluorescence Sensing by a Functionalized Mesoporous Material Covalently Grafted with a Fluorescent Chromophore and Consequent Biological Applications. *Adv. Funct. Mater.* 19, 223–234. doi:10.1002/adfm.200800888
- Srivastava, T., Haq, W., and Katti, S. B. (2001). Carbodiimide Mediated Synthesis of 4-thiazolidinones by One-Pot Three-Component Condensation. *Tetrahedron* 58, 7619–7624. doi:10.1016/S0040-4020(02)00866-9
- Tamami, B., Allahyari, H., Ghasemi, S., and Farjadian, F. (2011). Palladium Nanoparticles Supported on Poly (N-Vinylpyrrolidone)-Grafted Silica as New Recyclable Catalyst for Heck Cross-Coupling Reactions. *J. Organomet. Chem.* 696, 594–599. doi:10.1016/j.jorganchem.2010.09.028
- Tamoradi, T., Daraie, M., and Heravi, M. M. (2020). Synthesis of Palladated Magnetic Nanoparticle (Pd@Fe<sub>3</sub>O<sub>4</sub>/AMOCOA) as an Efficient and Heterogeneous Catalyst for Promoting Suzuki and Sonogashira Cross-Coupling Reactions. *Appl. Organometal. Chem.* 34, e5538. doi:10.1002/aoc.5538
- Tamoradi, T., Daraie, M. M., Heravi, M. M., and Karmakar, B. (2020). Erbium Anchored Iminodiacetic Acid (IDA) Functionalized CoFe<sub>2</sub>O<sub>4</sub> Nano Particles: An Efficient Magnetically Isolable Nanocomposite for the Facile Synthesis of 1,8-naphthyridines. *New J. Chem.* 44, 11049–11055. doi:10.1039/D0NJ01676D
- Thakare, M. P., Kumar, P., Kumar, N., and Pandey, S. K. (2014). Silica Gel Promoted Environment-Friendly Synthesis of 2,3-disubstituted 4-thiazolidinones. *Tetrahedron Lett.* 55, 2463–2466. doi:10.1016/j.tetlet.2014.03.007
- Thakare, M. P., Shaikh, R., and Tayade, D. (2016). Catalyst-free and Environment Friendly Synthesis of 2-Aryl-3-Substituted-4-Thiazolidinones in Water. *RSC Adv.* 6, 28619–28623. doi:10.1039/C6RA02064J
- Ulusal, F., and Güzel, B. (2018). Deposition of Palladium by the Hydrogen Assisted on SBA-15 with a New Precursor Using Supercritical Carbon Dioxide. *J. Supercrit. Fluids* 133, 233–238. doi:10.1016/j.supflu.2017.10.023
- Veisi, H., Mohammadi, L., Hemmati, S., Tamoradi, T., and Mohammadi, P. (2019). *In Situ* immobilized Silver Nanoparticles on *Rubia Tinctorum* Extract-Coated Ultrasmall Iron Oxide Nanoparticles: An Efficient Nanocatalyst with Magnetic Recyclability for Synthesis of Propargylamines by A<sup>3</sup> Coupling Reaction. *ACS Omega* 4, 13991–14003. Available at: <http://pubs.acs.org/journal/acsofd>.
- Veisi, H., Ozturk, T., Karmakar, B., Tamoradi, T., and Hemmati, S. (2020). *In Situ* decorated Pd NPs on Chitosan-Encapsulated Fe<sub>3</sub>O<sub>4</sub>/SiO<sub>2</sub>-NH<sub>2</sub> as Magnetic Catalyst in Suzuki-Miyaura Coupling and 4-nitrophenol Reduction. *Carbohydr. Polym.* 235, 115966. doi:10.1016/j.carbpol.2020.115966
- Veisi, H., Tamoradi, T., Karmakar, B., and Hemmati, S. (2020). Green tea Extract-Modified Silica Gel Decorated with Palladium Nanoparticles as a Heterogeneous and Recyclable Nanocatalyst for Buchwald-Hartwig C–N Cross-Coupling Reactions. *J. Phys. Chem. Sol.* 138, 109256. doi:10.1016/j.jpics.2019.109256
- Veisi, H., Tamoradi, T., Karmakar, B., Mohammadi, P., and Hemmati, S. (2019). *In Situ* biogenic Synthesis of Pd Nanoparticles over Reduced Graphene Oxide by Using a Plant Extract (Thymra Spicata) and its Catalytic Evaluation towards Cyanation of Aryl Halides. *Mater. Sci. Eng. C.* 104, 109919. doi:10.1016/j.msec.2019.109919
- Wan, Y., and Zhao, D. (2007). On the Controllable Soft-Templating Approach to Mesoporous Silicates. *Chem. Rev.* 107, 2821–2860. doi:10.1021/cr068020s
- Zhang, H., Zhang, J., Qu, W., Xie, S., Huang, L., Chen, D., et al. (2020). Design, Synthesis, and Biological Evaluation of Novel Thiazolidinone-Containing Quinoxaline-1,4-Di-N-Oxides as Antimycobacterial and Antifungal Agents. *Front. Chem.* 8, 598. doi:10.3389/fchem.2020.00598
- Zhao, D., Feng, J., Huo, Q., Melosh, N., Fredrickson, G. H., Chmelka, B. F., et al. (1998). Triblock Copolymer Syntheses of Mesoporous Silica with Periodic 50 to 300 Angstrom Pores. *Science* 279, 548–552. doi:10.1126/science.279.5350.548

**Conflict of Interest:** The authors declare that the research was conducted in the absence of any commercial or financial relationships that could be construed as a potential conflict of interest.

**Publisher's Note:** All claims expressed in this article are solely those of the authors and do not necessarily represent those of their affiliated organizations, or those of the publisher, the editors, and the reviewers. Any product that may be evaluated in this article, or claim that may be made by its manufacturer, is not guaranteed or endorsed by the publisher.

Copyright © 2021 Kalhor and Dadras. This is an open-access article distributed under the terms of the Creative Commons Attribution License (CC BY). The use, distribution or reproduction in other forums is permitted, provided the original author(s) and the copyright owner(s) are credited and that the original publication in this journal is cited, in accordance with accepted academic practice. No use, distribution or reproduction is permitted which does not comply with these terms.